Chapter 2
Optical Properties of Nanocomposites Containing Metal Nanoparticles

Interaction of light with nanocomposites reveals novel optical phenomena indicating unrivalled optical properties of these materials. The linear and non-linear optical response of metal nanoparticles is specified by oscillations of the surface electrons in the Coulomb potential formed by the positively charged ionic core. This type of excitation is called the Surface Plasmon (SP). In 1908 Mie [1] proposed a solution of Maxwell's equations for spherical particles interacting with plane electromagnetic waves, which explains the origin of surface plasmon resonance (SPR) in the extinction spectra and colouration of metal colloids.

During the last century optical properties of nanoparticles have extensively been studied and metal-dielectric nanocomposites have found various applications in different fields of science and technology [2–6]. Since the optical properties of metal nanoparticles are governed by SPR, they are strongly dependent on the nanoparticles' size, shape, concentration and spatial distribution as well as on the properties of the surrounding matrix. Control over these parameters enables such metal-dielectric nanocomposites to become promising media for development of novel non-linear materials, nanodevices and optical elements.

In this section the SPR and main optical properties of metal nanoparticles embedded in a dielectric medium will be considered. A comprehensive review of the optical properties of nanostructured random media can be found in Refs. [7, 8].

2.1 Surface Plasmon Resonance of Isolated Metal Nanoparticles

Exposure of a metal nanoparticle to an electric field results in a shift of the free conduction electrons with respect to the particle's metal ion-lattice. The resulting surface charges of opposite sign on the opposite surface elements of the particles (see Fig. 2.1) produce a restoring local field within the nanoparticle, which rises with the increasing shift of the electron gas relative to the ionic background. The coherently shifted electrons of the metal particle together with the restoring field

A. Stalmashonak et al., *Ultra-Short Pulsed Laser Engineered Metal–Glass Nanocomposites*, SpringerBriefs in Physics,
DOI: 10.1007/978-3-319-00437-2_2, © The Author(s) 2013

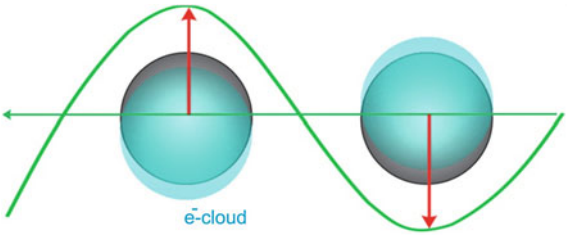

Fig. 2.1 Plasmon oscillations in metal spheres induced by an electromagnetic wave

consequently represent an oscillator, whose behavior is defined by the electron density and the geometry of the particle. Throughout this text the nanoparticles' resonances are called surface plasmons on metal nanoparticles.

An exact analytical, theoretical description of SPs of spherical metal nanoparticles is part of Mie's theory for scattering and absorption of light by spheres [7, 9]. According to the theory, different eigenmodes of the spherical particles are dipolar or multipolar in character. For particles that are small compared to the local variations of the involved electromagnetic fields, the quasi-static approximation is valid [7]. It assumes the exciting field to be homogeneous and not retarded over the particle's volume. Under these assumptions, the results of electrostatics can be applied by using the corresponding frequency dependent dielectric function. In this case, the polarizability α and induced dipole moment p of a metal sphere embedded in dielectric are given as [10]:

$$\alpha = 4\pi R^3 \frac{\varepsilon_i(\omega) - \varepsilon_h}{\varepsilon_i(\omega) + 2\varepsilon_h}, \tag{2.1}$$

$$\vec{p}(\omega) = \alpha\varepsilon_0\vec{E}_0(\omega) = 4\pi\varepsilon_0 R^3 \frac{\varepsilon_i(\omega) - \varepsilon_h}{\varepsilon_i(\omega) + 2\varepsilon_h}\vec{E}_0(\omega), \tag{2.2}$$

where R is the radius of the nanoparticle, E_0 the electric field strength of the incident electromagnetic wave, ε_0 the electric permittivity of vacuum, and $\varepsilon_i(\omega)$ and ε_h are the relative complex electric permittivity of the metal and host matrix respectively.

The absorption cross-section of a spherical metal inclusion placed in a transparent dielectric matrix, where the imaginary part of the relative complex electric permittivity approaches zero ($\mathrm{Im}[\varepsilon_h] \to 0$), is then given as:

$$\sigma(\omega) = 12\pi R^3 \frac{\omega}{c}\varepsilon_h^{3/2} \frac{\varepsilon_i''(\omega)}{\left[\varepsilon_i'(\omega) + 2\varepsilon_h\right]^2 + \varepsilon_i''(\omega)^2} \tag{2.3}$$

where $\varepsilon_i'(\omega)$ and $\varepsilon_i''(\omega)$are the real and imaginary parts of the electric permittivity of the metal, which in turn can be described by the Drude-Sommerfeld formula:

$$\varepsilon_i(\omega) = \varepsilon_b + 1 - \frac{\omega_p^2}{\omega^2 + i\gamma\omega}. \tag{2.4}$$

Here, γ is the damping constant of the electron oscillations and ε_b is the complex electric permittivity associated with interband transitions of the core electrons in the atom. The free electron plasma frequency is given by:

$$\omega_p = \sqrt{\frac{Ne^2}{m\varepsilon_0}}, \tag{2.5}$$

where N is the density of the free electrons and m is the effective mass of an electron.

As can be seen from Eqs. 2.1–2.3, the well-known Mie resonance occurs at the SP frequency ω_{SP} under the following conditions:

$$\left[\varepsilon_i'(\omega) + 2\varepsilon_h\right]^2 + \varepsilon_i''(\omega)^2 \rightarrow Minimum. \tag{2.6}$$

If the imaginary part of the metal electric permittivity is small in comparison with $\varepsilon_i'(\omega)$, or has small frequency dependence, then Eq. 2.6 can be written as:

$$\varepsilon_i'(\omega_{SP}) = -2\varepsilon_h. \tag{2.7}$$

Thus, if the condition represented in Eq. 2.7 is fulfilled, the dipole moment and local electric field in the vicinity of the nanosphere grow resonantly and can achieve magnitudes enhanced by many orders, overcoming the field of the incident wave. This phenomenon is responsible for the SP enhanced non-linearities in metal colloids.

Equation 2.7 requires the real part of the dielectric function of metals to be negative. This is indeed the case for noble metals in the visible spectral region (as an example see Fig. 2.2 for Ag). For a silver nanoparticle surrounded by a dielectric environment with $\varepsilon_h = 2.25$, the resonance condition is observed to occur at around 400 nm (Fig. 2.3). This results in the observation of bright colours both in transmitted and reflected light from such a medium.

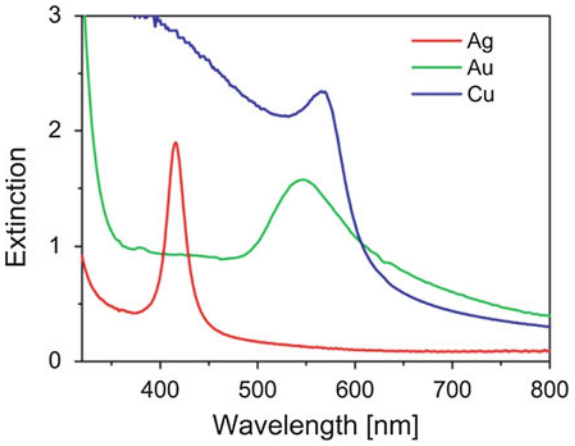

Fig. 2.2 Extinction spectra of glass containing *spherical silver*, *gold* and *copper* nanoparticles

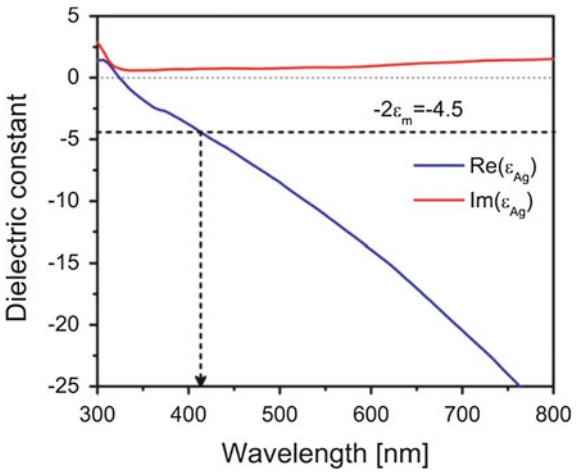

Fig. 2.3 The dielectric function of silver (*solid lines* data adapted from Ref. [11]): comparing its real part to $-2\varepsilon_m$ (*dashed line*) of an idealized dielectric medium with a wavelength independent dielectric constant of $\varepsilon_m = 2.25$ ($n = 1.5$), the surface plasmon resonance condition is found at $\sim$410 nm (*vertical arrow*)

Using Eq. 2.7 and by substituting the real part of the metal electric permittivity from Eq. 2.4, the position of the SP resonance can be expressed as follows:

$$\omega_{SP}^2 = \frac{\omega_p^2}{\mathrm{Re}[\varepsilon_b] + 1 + 2\varepsilon_h} - \gamma^2. \tag{2.8}$$

Core electrons have a significant influence on the SP and define the position of the SPR in the extinction spectra (Fig. 2.2) for different noble metals. For instance, silver nanoparticles embedded in glass matrix exhibit a SP band at about 415 nm. In turn, SP for Au and Cu nanoparticles is shifted in the red spectral range and peaked at 528 and 570 nm, respectively. The broad absorption bands below 500 nm for both Au- and Cu-containing nanocomposite glasses are associated with interband transitions, namely from the *d*- to *s*-shell, of the core electrons in the metal atoms. However, for silver the interband resonance is peaked at 310 nm (4 eV), far away from the SP resonance [11].

On the other hand, Eq. 2.8 qualitatively describes a dependence of the SP resonance on the dielectric properties of the host matrix, which the metal nanoparticles are incorporated in. An increase of dielectric constant (refractive index) evokes a shift of absorption maximum towards longer wavelengths [7, 12, 13] (as would be expected from Fig. 2.3). Figure 2.4 represents the spectral positions of SPRs of silver nanoparticles embedded in vacuum ($\varepsilon_h = 1$) and glass ($\varepsilon_h = 2.25$). It is clearly seen that the SP resonance maxima are more red-shifted for nanocomposites having a matrix with higher dielectric constant.

Figure 2.4 also shows that the position of the SPR depends on the size of metallic nanoparticles. In fact, its position remains quasi-constant for nanoparticles with radii smaller than 10–15 nm, while the band's half-width for these clusters differs by a factor of 4. This is often described as an intrinsic size effect [7, 14, 15]. If the particle size is below the dimension of the mean free path of the electrons in the metal ($\approx$10–15 nm) [16], the electron scattering at the particle surface mainly

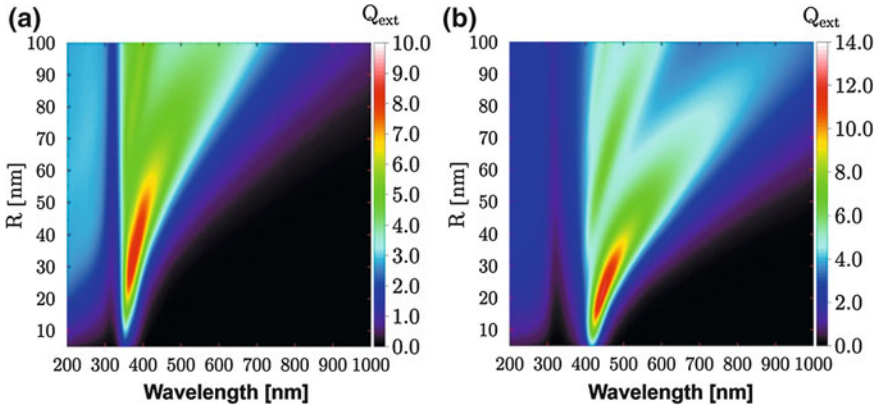

Fig. 2.4 Extinction spectra of spherical silver nanoparticles in **a** vacuum and **b** glass as a function of particle size

increases the imaginary part of the dielectric function. For the smaller particles (>1 nm) the spill-out of electrons from the particle surface should be taken into account, which results in an inhomogeneous dielectric function. As a result of this effect, very broad plasmon bands are observed for small nanoparticles (not included in Fig. 2.4).

The SPR shifts towards longer wavelengths with a simultaneous increase in the band half-width for nanospheres with radii larger than 15 nm (Fig. 2.4). This effect for the larger particle is referred to as an extrinsic size effect [7, 14, 17–19]. In this case, higher-order (such as quadrupolar) oscillations of conduction electrons become important.

From the size dependence of the SP, it is quite obvious that metal nanoparticles with non-spherical shape will show several SP resonances in their spectra. For instance, ellipsoidal particles with axes a ≠ b ≠ c own three SP modes corresponding to polarizabilities along the principal axes given as:

$$\alpha_k(\omega) = \frac{4\pi}{3} abc \frac{\varepsilon_i(\omega) - \varepsilon_h}{\varepsilon_h + (\varepsilon_i(\omega) + \varepsilon_h) L_k}, \tag{2.9}$$

where L_k is the geometrical depolarization factor for each axis ($\Sigma L_k = 1$). Moreover, an increase in the axis length leads to the minimization of the depolarization factor. For a spherical particle $L_a = L_b = L_c = 1/3$.

Thus, if the propagation direction and polarization of the electromagnetic wave do not coincide with the axes of the ellipsoid, the extinction spectra can demonstrate three separate SP bands corresponding to the oscillations of the free electrons along these axes [7]. For spheroids one has: $a \neq b = c$, and the spectra exhibit *two* SP resonances. However, if the incident light is polarized parallel to one of the axes, only one single SP band corresponding to the appropriate axis is observed (Fig. 2.5). The band lying at higher wavelengths is referred to as the long axis, while the small axis demonstrates resonance at shorter wavelengths compared

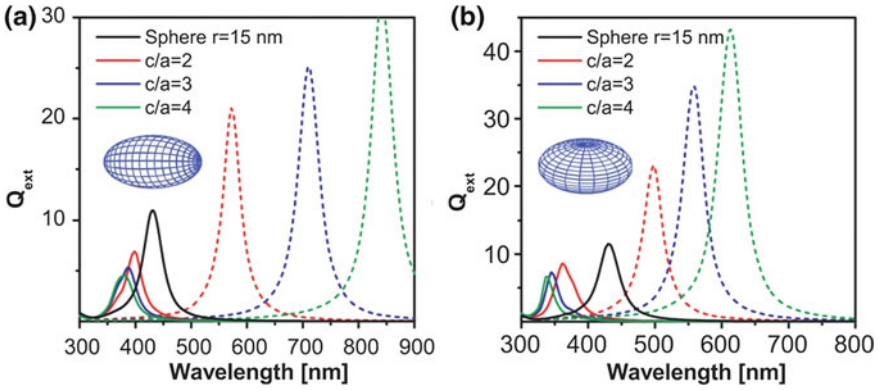

Fig. 2.5 Calculated using the Mie theory for spheroids [22], polarized extinction spectra are shown for **a** prolate and **b** oblate silver spheroids with different aspect ratios, which are embedded in glass. The volume of the spheroids is equal to the volume of a nanosphere with radius of 15 nm. *Dashed curves* polarization of the light is parallel to the long axis; *solid lines* parallel to the short axis. The insets schematically show the shape of the spheroids

to the single resonance of a nanosphere of the same volume. The spectral separation of the two surface plasmon bands of the ellipsoidal nanoparticle strongly depends on its aspect ratio [20, 21], which is defined as the ratio of the long to the short axes. At the same time, it is clearly seen that for prolate and oblate spheroids having the same aspect ratio, the positions of SP resonances are different. Namely, the spectral separation between SP bands is higher for the nanoparticles having a zeppelin-like shape.

For many years now, the dichroic property of elongated metallic nanoparticles has been used for manufacture of broad-band high-contrast polarizers [22]. This became possible because the position of the SP resonance can be designed within a broad spectral range by an appropriate choice of aspect ratio between the axes of the nanoparticles. This aspect will be discussed in more detail in the next sections.

2.2 Optical Properties of Nanocomposites with a High Fraction of Metal Nanoparticles

Increasing the volume fraction of metal nanoparticles in a medium leads to a decrease in the average inter-particle distances. Thus, enhancement of the dipole moment of spherical metal NPs by excitation near to their SP resonance results in strong collective dipolar interactions between the nanoparticles, which in turn affect the linear and non-linear optical properties of the nanocomposite material. For the purpose of this work it is sufficient to describe these effects using the approximation of the well-known Maxwell–Garnett effective medium theory. This theory is widely applied to describe the optical properties of metal particles in

dielectric matrices [8, 9, 23, 24]. The theory does not correctly take into account the multipolar interactions between nanoparticles considered in other works [25, 26]. However, it describes quite well the position and shape of the SP resonance and its dependence on the metal filling factor [8].

The effective dielectric constant $\varepsilon_{eff}(\omega)$ of a composite material with spherical metal inclusions having a filling factor f (volume of the silver inclusions per unit volume of the composite material $f = V_{Ag}/V_{total}$) is given by the expression:

$$\varepsilon_{eff}(\omega) = \varepsilon_h \frac{(\varepsilon_i(\omega) + 2\varepsilon_h) + 2f(\varepsilon_i(\omega) - \varepsilon_h)}{(\varepsilon_i(\omega) + 2\varepsilon_h) - f(\varepsilon_i(\omega) - \varepsilon_h)}, \tag{2.10}$$

where $\varepsilon_i(\omega)$ and ε_h are the complex electric permittivities of the metal (given by the Eq. 2.4) and the host matrix, respectively. Based on this description, the complex index of refraction of a composite medium can be defined as

$$n(\omega) = n' + in'' = \sqrt{\varepsilon_{eff}(\omega)}. \tag{2.11}$$

Hence, the absorption coefficient α and refractive index n' of the medium with dielectric constant $\varepsilon_{eff}(\omega)$ can be expressed as

$$\alpha = \frac{2\omega}{c} \mathrm{Im}\sqrt{\varepsilon_{eff}(\omega)}, \tag{2.12}$$

$$n'(\omega) = \mathrm{Re}\sqrt{\varepsilon_{eff}(\omega)}, \tag{2.13}$$

where c is the light velocity. Using Eqs. 2.10–2.13, the absorption cross-section and dispersion spectra (Fig. 2.6a, b) of glass containing spherical silver nanoparticles can be calculated as a function of the volume filling factor of the metal clusters in the glass matrix, using: $\varepsilon_h = 2.3$, $\omega_p = 9.2$ eV, $\gamma = 0.5$ eV [27], $\varepsilon_b = 4.2$ [24].

The collective dipolar interactions between nanoparticles cause a broadening and red-shift of the absorption band with increasing filling factor of the inclusions in the glass matrix (Fig. 2.6a). The effective refractive index of the composite glass also changes with growing filling factor (Fig. 2.6b)—at low content of silver nanoparticles in glass ($f = 0.001$) the refractive index is identical to that of clear glass ($n' = 1.52$), higher filling factors result in significant modifications of the dispersion spectra. For $f = 0.1$, the refractive index varies between ~ 1.2 and 2.1 on different sides of the SP resonance. As shown in Fig. 2.6c, the reflectivity R—given for normal incidence by:

$$R(\omega) = \left|\frac{n(\omega) - 1}{n(\omega) + 1}\right|^2 \tag{2.14}$$

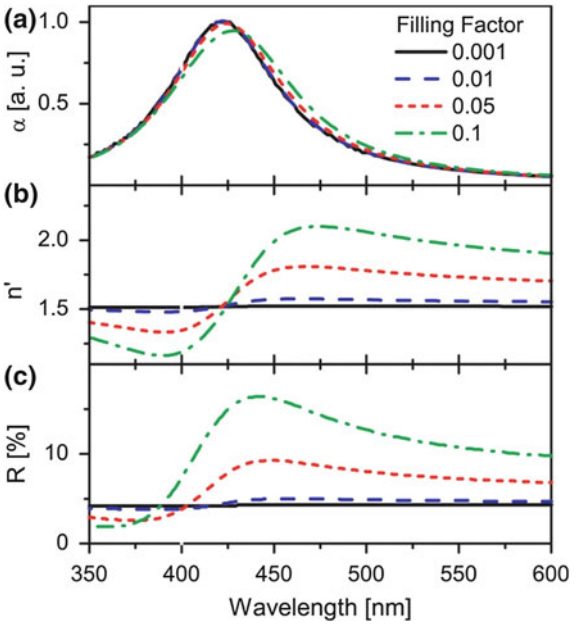

Fig. 2.6 **a** Absorption cross-section, **b** dispersion and **c** reflection spectra of composite glass containing Ag nanoparticles calculated according to the Maxwell–Garnett theory

also changes upon increasing the volume filling factor. In particular, in the visible range the main effect is an increase in reflectivity of the composite medium with an increasing content of nanoparticles.

2.3 Preparation and Characterization of Glass Samples Containing Silver Nanoparticles

The samples were prepared from soda-lime float glass (72.5 SiO_2, 14.4 Na_2O, 0.7 K_2O, 6.1 CaO, 4.0 MgO, 1.5 Al_2O_3, 0.1 Fe_2O_3, 0.1 MnO, 0.4 SO_3 in wt %) by Ag^+–Na^+ ion exchange. For the ion exchange process the glass substrate is placed in a mixed melt of $AgNO_3$ and KNO_3 at 400 °C [12, 28]. The thickness of the glass substrate, time of the ion exchange process and weight concentration of $AgNO_3$ in the melt determine the concentration and distribution of Ag^+ ions in the glass. Subsequent thermal annealing of the ion exchanged glass in an H_2 reduction atmosphere, typically at 400–450 °C, results in the formation of spherical silver NPs [12]. As could be expected, size and depth distribution of the Ag NPs in the glass sample strongly depend on the temperature and duration of the Na–Ag ion exchange as well as on the duration of the annealing. In our case, the spherical Ag NPs of 30–40 nm in mean diameter (Fig. 2.7a) are distributed in a thin surface layer of approximately 6 μm thickness (with total thickness of the glass plate being 1 mm).

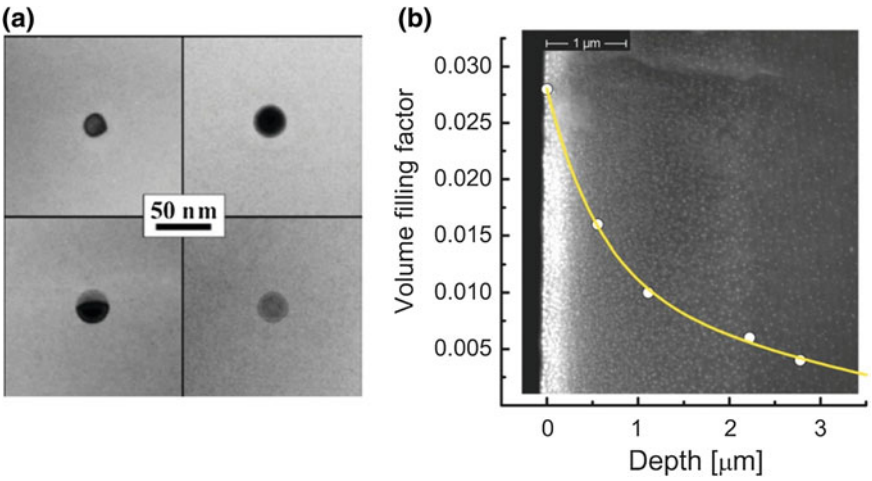

Fig. 2.7 **a** TEM image of typical spherical silver nanoparticles in nanocomposite glass. **b** SEM image of the cross-section of a glass sample containing spherical silver nanoparticles (Ag particles are reproduced as *white spots*). The gradient of the volume filling factor of Ag nanoparticles is shown superimposed (the x-axis was adjusted to the length scale of the image)

The scanning electron microscopy (SEM) image of the cross-section of the nanocomposite is shown in Fig. 2.7b, where silver particles are reproduced as white spots. In order to obtain information on the depth distribution of silver NPs in the glass, surface layers of various thicknesses were removed from the sample by etching in 12 % HF acid for different retention times. After this procedure SEM images were recorded for all etched surfaces [e.g., Fig. 2.8a, increasing etching time from (i) to (iv)], as well as optical extinction spectra (see Fig. 2.8b). The area fraction of silver derived from the SEM images was then converted to a volume fill factor assuming a typical electron penetration depth of 500 nm. The result is given as the superimposed curve in Fig. 2.7b, showing the highest silver content of $f = 0.028$ directly below the glass surface. Within a few micrometers the fill factor then strongly decreases with increasing distance from the surface.

Figure 2.8b depicts the corresponding extinction spectra with the same lettering as in Fig. 2.8a. However, it should be noticed that the optical spectra integrate over the whole particle-containing layer. Thus, for the original sample the absorption around SP resonance is very high, discouraging any detailed analysis of the spectral band shape. The same holds for extinction after the shortest etching time [Fig. 2.8b, curve (i)]; however, at least one can estimate for this case an extinction peak wavelength in the range of 420–440 nm. Further etching of the sample results in a fading of the extinction band caused by the decrease in thickness of the silver-nanoparticle containing layer. Spectrum (i) indicates that the uppermost metal-rich layers are responsible for the shift observed in the red wing of the SP band towards longer wavelengths.

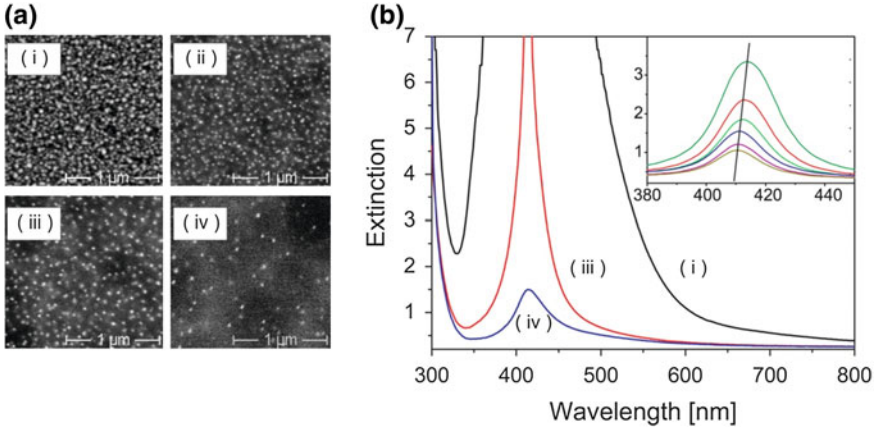

Fig. 2.8 **a** SEM images of etched samples showing Ag nanoparticles (volume fill factor: *i* 0.01, *ii* 0.006, *iii* 0.004, *iv* 0.001). **b** Extinction spectra of samples with spherical silver nanoparticles after different times of etching in 12 % HF acid. Labeling of the spectra is according to the SEM images shown in (**a**). The samples with lower fill factor exhibit lower extinction

Etching the samples for longer times, so that one ends up at a residual filling factor of less than 0.004, leads to an easily measurable extinction spectrum. The corresponding evolution of the spectra with etching time is shown in more detail in the inset of Fig. 2.8b. It is seen that a decrease of filling factor (by longer time of etching) leads to a slight shift of the SP band maxima to shorter wavelengths. This is compatible with the Maxwell–Garnett theory, which predicts a red-shift of the SP band for the samples with higher filling factors [7, 8, 29].

It should be mentioned here that for the study of the basic physical processes of nanoparticle shape transformation, etched samples with a maximum Ag filling factor of 10^{-3} were used, where the NPs are, to good approximation, understood as non-interacting (isolated) nanoparticles. However, the experiments related to the maximization of polarization contrast were performed on samples with considerably higher filling factor ($f \sim 0.01$).

References

1. Mie, G.: Beiträge zur Optik trüber Medien, speziell kolloidaler Metallösungen. Ann. Phys. **25**, 377–445 (1908)
2. Shalaev, V.M., Kawata, S.: Nanophotonics with surface plasmons. Advances in Nano-Optics and Nano-Photonics. Elsevier, UK (2007)
3. Brongersma, M L.; Kik, P G. Surface Plasmon Nanophotonics; Springer Series in OPTICAL SCIENCES 131; Springer: Berlin, DE, 2007
4. Tominaga, J., Tsai, D.P.: Optical Nanotechnologies: The Manipulation of Surface and Local Plasmons, Topics in Applied Physics, vol. 88. Springer, Berlin (2003)

5. Righini, M., Girard, C., Quidant, R.: Light-induced manipulation with surface plasmons. J. Opt. A: Pure Appl. Opt. **10**, 093001 (2008)
6. Wang, J., Blau, W.J.: Inorganic and hybrid nanostructures for optical limiting. J. Opt. A: Pure Appl. Opt. **11**, 024001 (2009)
7. Kreibig, U., Vollmer, M.: Optical Properties of Metal Clusters, Springer Series in Material Science, vol. 25. Springer, Berlin (1995)
8. Shalaev, V.M.: Optical Properties of Nanostructured Random Media, Topics in Applied Physics, vol. 82. Springer, Berlin (2002)
9. Bohren, C.F., Huffman, D.R.: Absorption and Scattering by Small Particles. Wiley, New York (1983)
10. Maier, S.A.: Plasmonics: Fundamentals and Applications. Springer, Berlin (2007)
11. Kresin, V.V.: Collective resonances in silver clusters: Role of *d* electrons and the polarizationRfree surface layer. Phys. Rev. B **51**, 1844–1899 (1995)
12. Berg, K.-J., Berger, A., Hofmeister, H.: Small silver particles in glass surface layers produced by sodium-silver ion exchange–their concentration and size depth profile. Z. Phys. D **20**, 309–311 (1991)
13. Hilger, A., Tenfelde, M., Kreibig, U.: Silver nanoparticles deposited on dielectric surfaces. Appl. Phys. B **73**, 361–372 (2001)
14. Link, S., El-Sayed, M.A.: Optical Properties and Ultrafast Dynamics of Metallic Nanocrystals. Ann. Rev. Phys. Chem. **54**, 331–366 (2003)
15. Berciaud, S., Cognet, L., Tamarat, P., Lounis, B.: Observation of Intrinsic Size Effects in the Optical Response of Individual Gold Nanoparticles. Nano Lett. **5**, 515–518 (2005)
16. Seah, M.P., Dench, W.A.: Quantitative electron spectroscopy of surfaces: A standard data base for electron inelastic mean free paths in solids. Surf. Interface Anal. **1**, 2–11 (1979)
17. Genzel, L., Martin, T.P., Kreibig, U.: Dielectric function and plasma resonances of small metal particles. Z. Phys. B **21**, 339–346 (1975)
18. Kreibig, U., Genzel, L.: Optical absorption of small metallic particles. Surf. Sci. **156**, 678–700 (1985)
19. Amendola, V., Meneghetti, M.: Size Evaluation of Gold Nanoparticles by UV−vis Spectroscopy. J. Phys. Chem. C **113**, 4277–4285 (2009)
20. Postendorfer, J.: Numerische Berechnung von Extinktions- und Streuspektren spharoidaler Metallpartikel beliebiger Größe in dielektrischer Matrix. PhD thesis, Martin-Luther University Halle-Wittenberg (1997)
21. Voshchinnikov, N.V., Farafonov, V.G.: Optical properties of spheroidal particles. Astrophys. Space Sci. **204**, 19–86 (1993)
22. See for example the following link: http://www.codixx.de/
23. Marton, J.P., Lemon, J.R.: Optical Properties of Aggregated Metal Systems. Phys. Rev. B **4**, 271–280 (1971)
24. Xu, G., Tazawa, M., Jin, P., Nakao, S.: Surface plasmon resonance of sputtered Ag films: substrate and mass thickness dependence. Appl. Phys. A **80**, 1535–1540 (2005)
25. Markel, V.A., Muratov, L.S., Stockman, M.I., George, T.F.: Theory and numerical simulation of optical properties of fractal clusters. Phys. Rev. B **43**, 8183–8195 (1991)
26. Markel, V.A., Shalaev, V., Stechel, E.B., Kim, W., Armstrong, R.L.: Small-particle composites. I. Linear optical properties. Phys. Rev. B **53**, 2425–2436 (1996)
27. Lamprecht, B., Leitner, A., Ausseneg, F.G.: Femtosecond decay-time measurement of electron-plasma oscillation in nanolithographically designed silver particles. Appl. Phys. B **64**, 269–272 (1997)
28. Hofmeister, H., Drost, W.G., Berger, A.: Oriented prolate silver particles in glass-characteristics of novel dichroic polarizers. Nanostruct. Mater. **12**, 207–210 (1999)
29. Gittleman, J.I., Abeles, B.: Comparison of the effective medium and the Maxwell-Garnett predictions for the dielectric constants of granular metals. Phys. Rev. B **15**, 3273–3275 (1977)

http://www.springer.com/978-3-319-00436-5

Ultra-Short Pulsed Laser Engineered Metal-Glass Nanocomposites

Stalmashonak, A.; Seifert, G.; Abdolvand, A.

2013, XII, 70 p. 38 illus., 36 illus. in color., Softcover
ISBN: 978-3-319-00436-5